INSTYTUT FIZYKI JĄDROWEJ
INSTITUTE OF NUCLEAR PHYSICS
ИНСТИТУТ ЯДЕРНОЙ ФИЗИКИ

KRAKÓW

RAPORT No 1120/PL

ELASTIC SCATTERING OF 120, 145 AND 172.5 MeV α–PARTICLES BY ^{12}C, ^{24}Mg AND ^{27}Al AND OPTICAL MODEL ANALYSIS

S. WIKTOR, C. MAYER–BÖRICKE, A. KISS
M. ROGGE, P. TUREK, H. DĄBROWSKI

KRAKÓW 1980

ELASTIC SCATTERING OF 120, 145 AND 172.5 MeV α-PARTICLES BY ^{12}C, ^{24}Mg AND ^{27}Al AND OPTICAL MODEL ANALYSIS

ROZPRASZANIE SPRĘŻYSTE CZĄSTEK α O ENERGIACH 120, 145 I 172.5 MeV NA JĄDRACH ^{12}C, ^{24}Mg I ^{27}Al ORAZ ANALIZA PRZY POMOCY MODELU OPTYCZNEGO

УПРУГОЕ РАССЕЯНИЕ α-ЧАСТИЦ С ЭНЕРГИЕЙ 120, 145 И 172.5 Мэв НА ^{12}C, ^{24}Mg И ^{27}Al И ЕГО АНАЛИЗ С ПОМОЩЬЮ ОПТИЧЕСКОЙ МОДЕЛИ

S. Wiktor*, C. Mayer-Böricke, A. Kiss, M. Rogge, P. Turek and H. Dąbrowski*

Institut für Kernphysik der Kernforschungsanlage Jülich, D-5170 Jülich, W. Germany

*/Institute of Nuclear Physics, Cracow

CRACOW
December 1980

NAKŁADEM INSTYTUTU FIZYKI JĄDROWEJ W KRAKOWIE
UL. RADZIKOWSKIEGO 152

Kopię kserograficzną, druk i oprawę wykonano w IFJ Kraków

Wydanie I *Zam. 291/80* *Nakład 40 egz.*

The 120, 145 and 172.5 MeV α-particle beams from JULIC were used to measure differential cross sections for elastic scattering on ^{12}C,[2] ^{24}Mg[3] and ^{27}Al[4] in the angular range from about 5° to 70° (c.m. system). The angular distributions were analysed extensively in terms of the optical model using a variety of potential forms. Apart from the parametrized forms of potential, as Woods-Saxon (WS) or rather $(WS)^{V}$[7] also a model independent representation of potential spline potential was employed. The analysis based on the parametrized forms of the potential made it possible to find the best fit parameter sets, which were then examined on their uniqueness and energy dependence. Emphasis was given to gaining informations on the radial shape of the potential.

1) *α
2) *H1*H2C
3) *H2*H6Mg
4) *H2*H7Al
5) 5deg
6) 70deg
7) (WS)sup(*n)

Wiązki cząstek α o energiach 120, 145 i 172.5 MeV uzyskane z cyklotronu JULIC były użyte do pomiarów różniczkowych przekrojów czynnych rozpraszania sprężystego na jądrach ^{12}C, ^{24}Mg i ^{27}Al w obszarze kątowym 5° do 70° (c.m.). Rozkłady kątowe zostały poddane wielostronnej analizie w ramach modelu optycznego z zastosowaniem różnych postaci potencjału. Oprócz postaci parametrycznej jak Woodsa-Saxona (WS) lub $(WS)^{V}$ zastosowano również reprezentację potencjału niezależnego od modelu (potencjał spline). Analiza bazująca na parametrycznej postaci potencjału umożliwiła znalezienie parametrów najlepszego dopasowania, które zostały następnie przebadane pod względem jednoznaczności i zależności energetycznej. Poświęcono dużo uwagi by uzyskać informacje odnośnie radialnej formy potencjału.

Пучки α-частиц с энергиями 120, 145 и 172,5 Мэв, ускоренные на Юлихском циклотроне, были использованы для измерений дифференциальных сечений упругого рассеяния на мишенях ^{12}C, ^{24}Mg и ^{27}Al в угловом интервале 5 - 70° (ц. м.). Угловые распределения были проанализированы с помощью оптической модели с использованием потенциалов различной формы. Кроме параметризованной формы потенциала вида Вудса-Саксона (WS) или точнее $(WS)^V$, было также применено представление независимое от модели (оптин потенциал). Параметры потенциала в форме Вудса-Саксона, с помощью которых было получено наилучшее согласие с экспериментальными данными, были затем исследованы на единственность и зависимость от энергии. Много внимания было уделено получению сведений о радиальной форме потенциала.

1. Introduction

Only a few experiments have been reported so far on α-elastic scattering at incident energies well above 120 MeV. In ref. 1) α-scattering data are presented for ^{12}C, ^{28}Si, Sn and Pb at 166 MeV, the Maryland group published data for ^{12}C, ^{40}Ca, $^{46,48,50}Ti$, ^{58}Ni, ^{90}Zr and ^{208}Pb at about 140 MeV (refs. 2,3,4,5), then the Jülich-Heidelberg group investigated α-scattering on ^{16}O, ^{12}C, ^{20}Ne and ^{28}Si (refs. 6,7) at energies around 150 MeV and later Groningen group (ref. 8) presented a comprehensive study of α-scattering on ^{90}Zr over the energy range from 40 up to 120 MeV.

Elastic scattering data are generally analysed in terms of the optical model. Since most reaction theories utilize distorted waves to describe scattering of the projectile from the target, the extraction of optical potentials from elastic scattering data is the necessary starting point for gaining informati on nuclear structure from reaction processes. Unfortunately, the extraction of optical potential parameters for composite particles suffers at lower incident energies from the well known ambiguities both discreate and continuous. It has been however, fairly well established during the past few years[2,3,4,9] that a unique parameter sets can be obtained for alpha particles if the elastic angular distributions are measured at sufficiently high incident energies and up to large enough scattering angles. Such scattering is characterized by the existence of the maximum deflection angle Θ_r (rainbow angle), beyond which the differential cross section exhibitis an almost exponential fall-off. The optical model parameter set providing an overall fit to such an elastic angular distribution, measured weel beyond Θ_r, does not suffer from discrete ambiguities. It has also been shown see for example ref. 2 that six free parameters appear to be necessary if the standard Woods-Saxon form of potential is used in the analysis of scattering of α-particles at higher incident energies.

This paper presents experimental angular distributions of

elastically scattered α-particles on ^{12}C, ^{24}Mg and ^{27}Al at incident energies of 120, 145 and 172.5 MeV and their optical model analysis. The aims of the investigation were: first, to extend the available experimental information for these light nuclei to higher incident energies, next, to provide consistent optical model parameter sets and to study their energy dependence on the basis of data all obtained at the same laboratory at identical experimental conditions. It was attempted to gain also information on the radial shape of the potential.

2. Experimental arrangement and results

The experiments were performed at the Julich Isochronous Cyclotron JULIC[10] using an energy analysed beam. Beam monitoring was accomplished by means of a Faraday cup located 4 m behind the scattering chamber and, additionally by a monitor detector. The beam was focussed on the target to a spot of less than 2 mm diameter. The targets used in the experiment were self supporting foils of natural ^{12}C and ^{27}Al and highly enriched ^{24}Mg, with thicknesses of around 3 mg/cm^2. The zero point of the absolute angular scale was determined to be better than 0.03°. This was estimated by the energy calibration of the two peaks of α-particles scattered on hydrogen in a $(CH)_x$ target.

The target and the detector telescopes were placed inside a 1 m diameter scattering chamber. The scattered particles were detected and identified by the detector telescopes operating in the usual ΔE-E mode. The ΔE detector were Si surface barrier counters while the E detectors were Ge(Li) diodes of the side entry type[11] produced in the detector laboratory of the Institute. The energy resolution in the particle spectra was about 150 keV. This was sufficient to separate the elastic peak from the first inelastic peak in all spectra.

Spectra were obtained for ^{24}Mg at 145 and 172.5 MeV and for ^{12}C and ^{27}Al at 120, 145 and 172.5 MeV incident α-energies

from about 5° to 70° (c.m.). The experimental angular distributions resulting from these measurements are shown in fig. 1 (points). They show a diffraction pattern at small angles and a rapid fall-off with weak structure at larger angles, which supports the conjecture of rainbow scattering[4].

The main uncertainties in the evaluation of the cross-sections were those due to the target thicknesses, beam current integration and solid angles. The error in absolute cross-section (common normalization error) is estimated to be less than 15 % for all three nuclei. The relative error is smaller than 10 %. Except for the data points at the largest angles, the errors resulting from the counting rate are smaller than the data points in fig. 1.

3. Optical model analysis with the Woods-Saxon potential

We began the analysis of the data using the standard Woods-Saxon (WS) form of potential with volume absorption:

$$U(r) = V_c(r,r_c) - V\cdot f(r,r_v,a_v) - i\,W\cdot f(r,r_w,a_w) \qquad 1)$$

where $f(r,r_1,a_1) = \left(1 + \exp\left[(r - r_1\,A^{1/3})/a_1\right]\right)^{-1}$ and $V_c(r,r_c)$ is the Coulomb potential of a uniformly charged sphere of radius $r_c\cdot A^{1/3}$. In accordance with refs. 1, 4) the value of 1.3 fm for the Coulomb radius r_c was used throughout these analyses. The advantage of the volume absorption over surface absorption in the potential form had been proved in earlier study[12].

In order to find the best optical model parameter sets the quantity:

$$\chi^2 = \frac{1}{N}\sum_{i=1}^{N}\left[\frac{\sigma(\theta_i) - \sigma_{exp}(\theta_i)}{\Delta\sigma_{exp}(\theta_i)}\right]^2 \qquad 2)$$

was minimized with $\sigma(\theta_i)$ being the calculated differential cross-section and $\sigma_{exp}(\theta_i)$ and $\Delta\sigma_{exp}(\theta_i)$ denoting the expe-

mental cross-section and errors at angle θ_i respectively. The calculations were performed by using Raynal's computer program MAGALI[13].

The analysis was initiated by testing the uniqueness of the potential parameters. For this purpose, a V-grid search was performed by fixing V at a number of different values in the range from about 80 to 190 MeV. The remaining five parameters (r_v, a_v, W, r_w, a_w) were allowed to vary in order to minimize χ^2. Several such V-grid searches were performed using different starting parameter sets, including also the additional case of a fixed r_v to make sure that no discrete potential family was missed. This procedure was employed in the analysis of all experimental data. The results are presented in fig. 2. On the left side of this figure are plotted the minimized values of χ^2 versus V, and on the right side are plott the corresponding values of χ^2 vs. r_v.

If the discrete potential ambiguities were present in the large V-range investigated, they should show up in the χ^2 vs. V plots of fig. 2 as additional minima as deep as the main minimum[9]. Since no such effect is apparent, we conclude that the potentials found for the χ^2 minima are unique for our high incident energies. These minima, however, correspond to lower quality fits and therefore do not provide a competing parameter set of another family. Similarly, as it has been practiced in refs. 4 and 9), test searches were performed in order to demonstrate that the large angle played a critical role in removing the discrete ambiguities. For those tests the experimental data sets were gradually truncated from the side of large angles. If the data were truncated at angles below 30° a new discrete family of parameters originated, which fitted the data equally well.

The optimum parameter sets corresponding to the χ^2 minima of fig. 2 are summarized in table 1. In this table are also listed the root mean square (rms) radii of interaction for the real part of potential, evaluated for these parameters according to the formula commonly used[14] in the case of a WS formfactor.

The differential cross-sections calculated from these potentials are displayed in fig. 1. With respect to the parameters in table 1, we want to emphasize that a large difference between the parameters r_v and r_w shows up in all cases, r_w being much larger than r_v. This feature is in accordance with the results of refs. 1, 2, 3, 4, 6, 7, 9, 21 . It seems therefore to be a general feature of α-scattering.

In order to examine the question of continuous ambiguities in the optical model parameters, the volume integrals J/4A (per projectile-target nucleon pair) for the real part of potential were evaluated using the formula given in ref.[15]. Their numerical values, corresponding to the optimum fit parameters, are given in table 1. As expected for a definite potential family, obtained from lower incident energy data[15], the volume integrals were found to be approximately constant within some range of V, and especially in the neighbourhood of the narrow minimum of χ^2 versus r_v. Outside these limits of constancy the J/4A value changes sharply. This V-range, together with the corresponding range of fluctuations of J/4A values , is given in table 2 for the nuclei and energies studied.

Another limitation for V-range can be inferred by the requirement of compatible fit quality. If we accept a limit of 20 % deviation of χ^2 from the minimum in χ^2 vs. V as a standard for comparable fits then the range of possible continuous ambiguities is considerably reduced as can be seen quantitatively from the last two columns of table 2.

Inspection of table 1 shows that the integral quantities such as the rms radii and the volume integrals for the real part of potential behave under change of energy as expected from the model, i.e. the rms radii remain almost constant and the volume integrals decrease sytematically with increasing incident energy. Slopes of -0.95 MeV fm^3/MeV and -0.84 MeV·fm^3/MeV of volume integrals is found for ^{27}Al and ^{12}C respectively. A change of the normalization of the cross section by about 20 % is reflected in a 5 % change in the values of the volume integral. Smith et al.[2] report a slope of -1.1 MeV·

·fm^3/MeV for ^{12}C using their own 139 MeV data and additional data taken by other groups at 104 and 166 MeV. In medium weight nuclei the slope of the volume integral is about 0.3 - 0.6 MeV fm^3/MeV[8, 16, 17]. Furthermore at constant incident energy the volume integrals for ^{12}C, ^{24}Mg and ^{27}Al scattering decreases considerably with increasing mass number (table 1). However, if the present results at 145 MeV and those of ref. 4) around 140 MeV are combined, no monotonic variation of the value of the volume integral with A can be established, in contrast to the suggestion in ref. 4). This can be seen from the J/4A-values for ^{24}Mg (E_α = 145 MeV) and ^{27}Al (E_α = 145 MeV), which are already smaller than that for ^{40}Ca (E_α = 142 MeV), in ref. 4). This anomaly may be understood by taking into account the fact that in contrast to the nuclei studied by Goldberg et al.[4] the ^{24}Mg and ^{27}Al nuclei are deformed. Therefore, it may be worthwhile to perform experiments on heavier target nuclei and to do coupled channel calculations in order to find out whether the parameters describing the elastic scattering within this framework would exhibit a smoother A-dependence of the volume integral. Such problems have been previously discussed in the case of α-scattering in the rare-earth region[18].

The existence of continuous ambiguities between the parameters of the potential makes it impossible to examine the energy dependence of individual parameters of the potential reliably. Therefore, although the six parameter search produces the best fits, it may give rise to irregular fluctuations in the nergy dependence of the parameters. For instance, from our analysis has emerged an increase of the parameter V and a decrease of the parameter r_v, when the energy increases (table 1). Such increase of V is of course unphysical and indicates an inadequate potential form. In sections 4 and 5 we consider therefore other potential forms.

In case of the WS potential we have performed additional analyse of the data, as is often practiced by the authors who examine the subject of energy dependence of the potential[8, 19, 20], by fixing the geometrical parameters. In the first step only

the parameter r_v was fixed; the value of r_v = 1.20 fm for ^{12}C and r_v= 1.23 fm for ^{27}Al, i.e. those being optimal for E_α = 145 MeV, were used. This approach resulted immediately in producing a decrease of the parameter V with incresing energy; however, the fits became markedly worse than the six parameter ones Upon fixing the remaining geometrical parameters the real potential depth decreased almost linearly with increasing energy of incident α-particles, but the fits became increasingly worse. Similar detarioration of fits when the geometry was fixed had also been observed in other works [8,20,21,22].

4. Modification of the WS form of potential

For many years the WS form of potential was commonly used as capable of giving a satisfactory reproduction of scattering data. The microscopic calculations, however, which developed in the last few years [8,23, 24,30,33,34] indicate that the true form of potential, especially in the surface and tail regions, differs from that of the WS type. Model independent representations in terms of the spline functions [8,25], or the Fourier-Bessel expansion of potential [26] have recently proved that a modification of the WS form of potential is necessary.

To account to some extent for the modification of potential form some authors have attempted to use the square [5, 8,14,16 17,20,27] or another adjustable power [28,29] of the WS form. In this chapter a systematic study of the optimum power of the WS form will be presented [12]. We examined a parametrized form of potential:

$$V(r) = V_c(r,r_c) - V \cdot f(r,r_v,a_v)^n - i\,W \cdot f(r,r_w,a_w)^m \qquad 3)$$

where n and m are adjustable powers and the other symbols have the same meaning as in formula 1. Our method differs slightly from that of Michel et al. [28] by allowing different geometrical parameters in the real and imaginary parts and by changing the powers n and m independently.

The analysis was initiated by putting n = m. The value of n was fixed to a series of values between 0.8 and 3.0 and all six parameters of the potential were allowed to vary until the lowest value of χ^2 was reached for a given n. This approach has shown that an increase of n is accompanied by an increase of all potential parameters. This can be explained easily since the rise of the power of the WS form makes it shallower in the surface region. This region however is mostly probed in the scattering of α -particles, hence, the requirement to fit the data with a shallower potential requires in turn the strength and the radii of the potential to be respectively larger. It appears that the potential parameters and the magnitudes of n are strongly correlated, thus giving rise to creation a new ambiguity.

The variation of χ^2 with n is displayed for different nuclei and different energies in fig. 3. Full lines correspond to n = m, i.e. to the same shapes of the real and imaginary part. The resulting χ^2 values correspond in every point to the set of parameters producing optimum fits to the experimental data. From this figure it is seen that in the majority of cases one gets an improvement of the fits if the value of n is chosen greater than one. In the case of the lowest energies, i.e. of 120 MeV for ^{12}C and ^{27}Al the values of n tend to increase monotonically with decreasing χ^2 however, the strength of the potential increases beyond reasonable limits. Moreover, it looks from fig. 3 as if the optimum power n and hence the radial form of the potential changed, when the target nuclei and the beam energy are changed. Obviously, a standard, optimum n for different targets and different energies can not be found. On the basis of these results one can not claim that the square of the WS form is more suitable than the WS form.

The solid lines in fig. 1 correspond to the fits with n = 2. Except for the largest angles, the differences between the fits, corresponding to WS and $(WS)^2$ forms, are neglibile. The unphysical energy dependence of V (section 3) remains resistant to the change of the WS into the $(WS)^2$ form of the potential.

To examine the problem whether the forms of the real and imaginary parts of potential are the same, the analysis based on formula 3 was continued varying only the value of n and keeping constant the value of m. The dashed lines in fig. 3 correspond to the case of m = 1. Since in some cases the dashed lines are below the full lines one can conclude from fig. 3 that from the point of view of the data analysis different forms of the re and imaginary parts are allowed and that each of them could vary independently with energy. Different forms of the real and imaginary part of the potential were considered also in some microscopic calculations[24, 30, 33, 34].

The question arises how the curves, displayed in fig. 3. are changed by experimental errors. This problem was examined by means of introducing artificially a systematic and a relative error into the experimental data. The systematic error was simulated by changing the normalization of experimental data, and the relative error was introduced by changing a little the error for the angles at which the counting rate was poor. Fig. 4 illustrates the effect of the change of normalization. As is seen from this figure, the shape of the curves and the positions of the minima are practically unaffected by the change of systematic error. As has been proved, however, the relative error influences seriously the shapes and positions of minima of the curves presented on fig. 3. Especially careful estimation of this error is needed at the points where the cross section changes rapidly with angle and at the large angles where the statistics is poor and the background is high. In view of these facts the conclusions, drawn from fig. 3, must be taken only as tentative and not much importance can be attached to them.

5. Model independent analysis (spline function method)

In order to avoid the constraints imposed by the parametrized form of the potential a model independent analysis of the scattering data has been performed. Among the other possibili-

ties[26, 31] we choosed the spline function method[8, 25] as having a large "elasticity" to accommodate the radial form of potential for structural effects and being capable to account for possible fluctuations in the potential strength and potential form with the change of incident energy. Similarly as in refs. 8 and 25) we represented the real part of the potential by 11 discrete values $V(r_i)$ $(i = 0, 1 \ldots 10)$ between 0 and 10 fm: whereas the imaginary part W(r) was represented by a WS form. In summary 14 parameters were searched simultaneously to achieve a minimum in the χ^2 value. The program OPTY[32] accomplished the interpolation of the potential between the specific radii by a smoothly varying function constructed from cubic polynomials. For calculation of the error band we prepared a special code OPTER. The extension of the error band is determined from mutual correlations between the parameters within the range imposed by the criterion $\chi^2 = \chi^2_{min} + 1$. Of great importance in gaining a true form of the potential and reasonable extension of the error band are the estimated experimental errors.

The model independent analysis generally resulted in considerably better fits than obtained in the analysis based on WS or $(WS)^2$ forms of the potential (table 3). In fig. 5 are illustrated the radial shapes of potential V(r) found by the spline analysis. Shaded lines in this figure represent the limits of the error band and the dashed lines correspond to the WS form of V(r) caloulated from the best fit parameters, given in table 1. It can be seen from this figure that the spline formfactor (full lines) and the WS formfactor (dashed lines) practically overlap in the radial range of 3 - 7 fm. In this range of radii the error band is narrow; it becomes broad outside of this range, where also appreciable deviations between the spline formfactor and the WS formfactor show up.

In table 3 are listed the integral quantities as the rms -radii of interaction and the volume integrals. It is seen from tables 1 and 3 that the differences in rms -radii, determined by both methods, does not exceed 6 %. The rms-radii obtained from the WS formfactor are almost constant when the energy is

varied, whereas these obtained from the spline method, exhibit uncorrelated variations with energy. This is evidently due to the poor determination of V(r) by the spline method in the centre and in the tail region. Accordingly, the volume integrals show a similarly irregular behaviour, determinad by the use of the spline function method.

Looking at fig. 5 one can understand, that by the use of the parametrized form of potential as WS or $(WS)^2$ we can always obtain good fits, because the radial form of potential in the sensitivity region can always be adjusted to resemble the shape of the potential, found by the spline method.

Conclusions

This work demonstrates the absence of discrete ambiguities in the real WS potential depth, when the energy of the bombarding partioles increases in the elastic scattering of α-particles on ^{12}C, ^{27}Al and ^{24}Mg; it was shown in addition how the continuous ambiguity in this potential can be restricted.

The analysis of elastic scattering in terms of an optical potential with the WS form has given satisfactory fits providing that six parameters are searched. The average quantities, as rms-radii and volume integrals, evaluated by use of optimum fit parameters, behave consistently with the change of incident energy i.e. the rms-radii remain approximately constant and the volume integrals decrease roughly linearly with increasing energy.

The model independent form of potential, expressed in terms of the spline functions, allowed us to describe succesfully the angular distributions of scattered α-particles. It has been shown, that the parametrized potential with optimized parameters lies generally inside a narrow error band of the spline potential. A relatively large extension of the sensitivity region (3 - 7 fm in our case) implies in turn a large extension of the continuous ambiguity range, thus individual parameters, such as V or r_v could not be determined uniquelly.

Attempts were also made to modify the parametrized WS form of potential in order to get more detailed information: on the radial shape, on possible energy and mass dependence of this shape and on its equality for the real and imaginary parts of potential. It was learned, however, that such fine details were especially sensitive to the accuracy of experimental data.

We thank Prof. A. Budzanowski and Prof. D.A. Goldberg for helpfull discuasions.

References

1. B. Tatischeff and I. Brissaud, Nucl. Phys. A155 (1970) 89.

2. S.M. Smith, G. Tibell, A.A. Cowely, D.A. Goldberg, H.G. Pugh W. Reichart and N.S. Wall, Nucl. Phys. A207 (1973) 273.

3. D.A. Goldberg, S.M. Smith, H.G. Pugh, P.G. Roos, and N.S. Wa Phys. Rev. C7 (1973) 1938.

4. D.A. Goldberg, S.M. Smith, and G.F. Burdzik, Phys. Rev. C10 (1974) 1362.

5. P.L. Roberson, D.A. Goldberg, N.S. Wall, L.W. Woo and H.L. Chen, Phys. Rev. Lett. 42 (1979) 54.

6. K.T. Knöpfle, G.J. Wagner, H. Breuer, M. Rogge and C. Mayer-Böricke, Phys. Rev. Lett. 35 (1975) 779.

7. K.T. Knöpfle, G.J. Wagner, A. Kiss, M. Rogge, C. Mayer-Böric and Th. Bauer, Phys. Lett. 64B (1976) 263.

8. L.W. Put and A.M.J. Paans, Nucl. Phys. A291 (1977) 93.

9. D.A. Goldberg and S.M. Smith, Phys. Rev. Lett. 29 (1972) 500.

10. C. Mayer-Böricke, Report of the Kernforschungsanlage Jülich, West Germany, JUL-665-KP 1970.

11. G. Riepe and D. Protić, Nucl. Instr. Meth. 101 (1972) 77; G. Riepe, D. Protić and J. Reich, Nucl. Instr. Meth. 124 (1975) 527; G. Riepe and D. Protić IEEE Transactions Nucl. Science, NS-22 (1975) 1.

12. S. Wiktor, C. Mayer-Böricke, A. Kiss, M. Rogge, P. Turek, Lecture Notes in Phys, edited by J. Ehlers et al.; 89; Springer-Verlag Berlin Heidelberg New York 1979, p. 315.

13. J. Raynal, Optical Model Program MAGALI, CEN Saclay, Boite Postale No. 2, 92 Gif-Sur-Yvette, France.

14. G.W. Greenlees, G.J. Pyle and Y.C. Tang, Phys. Rev. 171 (1968) 1127.

15. D.C. Weisser, J.S. Lilley, R.K. Hobbie and G.W. Greenless, Phys. Rev. C, 2 (1970) 544.

16. A. Budzanowski, H. Dąbrowski, L. Freindl, K. Grotowski, S. Micek, R. Płaneta, A. Strzałkowski, M. Bosman, P. Leleux, P. Macq, J.P. Meulders and C. Pirart, Phys. Rev. C17 (1978) 951.

17. Th. Delbar, Gh. Gregoire, G. Paiǒ, R. Ceuleneer, F. Michel, R. Vanderpoorten, A. Strzałkoweki, A. Budzanowski, H. Dąbrowski, K. Grotowski, S. Micek, R. Płaneta, Phys. Rev. C18 (1978) 1237.

18. N.K. Glendenning, D.L. Hendrie and O.N. Jarvis, Phys. Lett. 26B (1968) 131.

19. D.F. Jackson and R.C. Johnson, Phys. Lett. 49B (1974) 249.

20. H.H. Chang, B.W. Ridley, T.H. Braid, T.W. Conlon, E.F. Gibson and N.S.P. King, Nucl. Phys. A270 (1976) 413.

21. H. Eickhoff, D. Frekers, H. Löhner, K. Poppensieker, R. Santo, G. Gaul, C. Mayer-Böricke and P. Turek, Nucl. Phys. A252 (1975) 333.

22. L.W. Put and A.M.J. Paans, Phys. Lett. B49 (1974) 226.

23. A. Budzanowski, A. Dudek, K. Grotowski and A. Strzałkowski, Phys. Lett. 32B (1970) 431.

24. F.A. Brieva and J.R. Rook, Nucl. Phys. A291 (1977) 299, 317.

25. F. Michel and R. Vanderpoorten, Phys. Lett. 82B (1977) 183.

26. E. Friedman and C.J. Batty, Phys. Rev. C17 (1978) 34.

27. D.A. Goldberg, Phys. Lett. 55B (1975) 59.

28. F. Michel and R. Vanderpoorten, Phys. Rev. C16 1977 142.

29. H.P. Gubler, U. Kiebele, H.O. Meyer, G.R. Plattner and I. Sick, Phys. Lett. B74 (1978) 202.

30. Z. Majka, A. Budzanowski, K. Grotowski and A. Strzałkowski, Phys. Rev. C18 (1978) 114.

31. N.S. Wall, A.A. Cowley, R.C. Johnson, A.M. Kobos, Phys. Rev. C17 (1978) 1315.

32. H. Dąbrowski, R. Płaneta and A. Djaloeis, KFA Report Jül-1637 1980.

33. N. Vinh Mau, Phys. Lett. 71B (1977) 5.

34. A. Budzanowski, A. Dudek, K. Grotowski, Z. Majka and A. Strzałkowski, Particles and Nuclei 6 (1974) 97.

35. A. Budzanowski, C. Alderliesten, J. Bojowald, C. Mayer-Böricke, W. Oelert, P. Turek and S. Wiktor, KFA Annual Report 1977 p.1.

36. J.P. Didelez, C. Mayer-Böricke, W. Oelert, M. Rogge, P. Turek and S. Wiktor, Nucl. Phys. A318 (1979) 205.

Table 1

Target	E_α (MeV)	V (MeV)	r_v (fm)	a_v (fm)	W (MeV)	r_w (fm)	a_w (fm)	χ^2	rms-radius (fm)	J/4A (MeV·fm^3)
^{12}C	120	97.9	1.340	0.74	17.3	1.856	0.47	3.08	3.635	388
	145	111.2	1.200	0.80	15.8	1.883	0.50	1.25	3.656	370.
	172.5	112.8	1.140	0.82	16.8	1.822	0.53	1.47	3.657	347.
^{24}Mg	145	100.8	1.282	0.78	20.4	1.745	0.48.	3.52	4.075	325.
	172.5	111.0	1.178	0.85	23.4	1.626	0.62	3.48	4.112	308.
^{27}Al	120	101.4	1.318	0.74	20.2	1.679	0.56	12.5	4.117	328.
	145	107.1	1.230	0.79	19.7	1.632	0.62	5.44	4.098	304.
	172.5	109.8	1.163	0.81	21.7	1.548	0.70	5.98	4.047	278.

Optimum WS parameter sets corresponding to the minima in the χ^2 plots of fig. 2.

Table 2

Target	E_α (MeV)	V-range (MeV)	J/4A-range (MeV · fm^3)	V-range $\frac{\Delta\chi^2}{\chi^2_{min}} \leq 20\%$	r_v-range $\frac{\Delta\chi^2}{\chi^2_{min}} \leq 20\%$
^{12}C	120	80–106	382–392	89–106	1.25–1.41
	145	85–147	362–372	102–117	1.16–1.27
	172.5	100–175	340–350	108–126	1.06–1.18
^{24}Mg	145	81–152	310–325	95–107	1.22–1.33
	172.5	84–126	302–318	103–117	1.13–1.24
^{27}Al	120	84–117	312–328	90–118	1.15–1.39
	145	79–114	300–318	97–120	1.10–1.31
	172.5	84–131	266–278	99–127	1.03–1.23

Ranges of fluctuations of volume integrals J/4A (under the requirement that they are approximately constant) and corresponding V parameter ranges for WS type analysis. In columns 5 and 6 are given the reduced ranges of V and r_v under the additional requirement of $\Delta\chi^2/\chi^2_{min} \leq 20\%$.

Table 3

Target	E_α (MeV)	rms-radius (fm)	J/4A (MeV·fm^3)	χ^2
^{12}C	120	3.61 ± 0.10	347. ± 12.	1.90
	145	3.62 0.06	376. 8.	0.66
	172.5	3.55 0.12	330. 12.	1.08
^{24}Mg	145	4.03 0.07	321. 7.	0.77
	172.5	4.12 0.10	310. 13.	1.82
^{27}Al	120	3.87 0.05	298. 9.	3.72
	145	4.09 0.13	300. 11.	3.35
	172.5	3.93 0.13	271. 10.	3.49

The rms radii of interaction, the volume integrals and χ^2-values resulting from the spline function calculations.

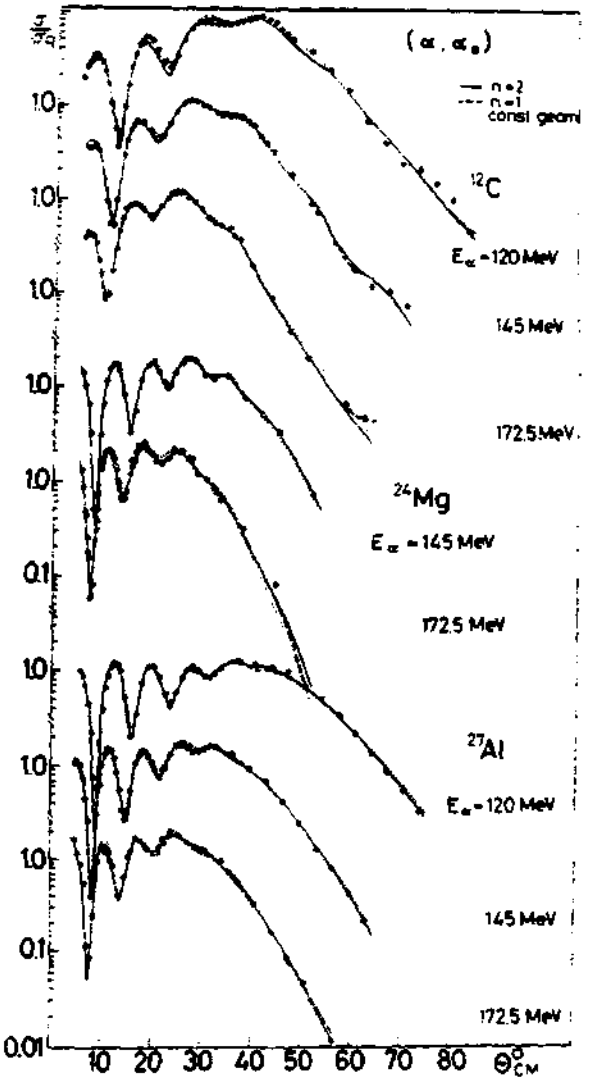

Fig. 1. Elastic α-scattering cross section normalized to the Rutherford cross section. Solid lines represent the 6-parameter $(WS)^2$ fits, dashed lines represent the 6-parameter WS fits and dotted lines represent the 2-parameter WS fits with constant geometry.

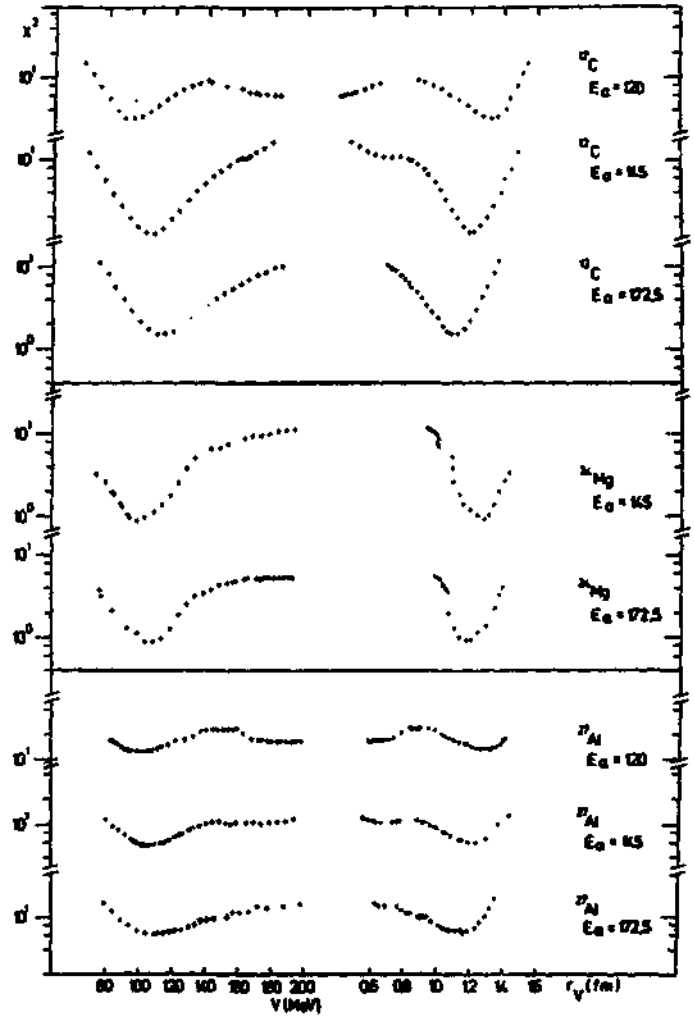

Fig. 2. The minimized values of χ^2 vs. V (left side) and χ^2 vs. r_V (right side) using a WS type potential.

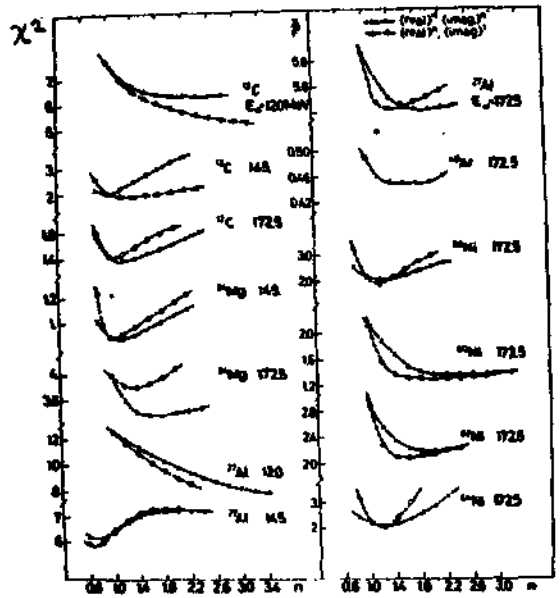

Fig. 3. The dependence of χ^2 on the power n. Solid lines correspond to n=m and dashed lines correspond to m constant (m=1). The data for ^{40}Ar and $^{58-64}Ni$ were taken from refs. 35 and 36 respectively.

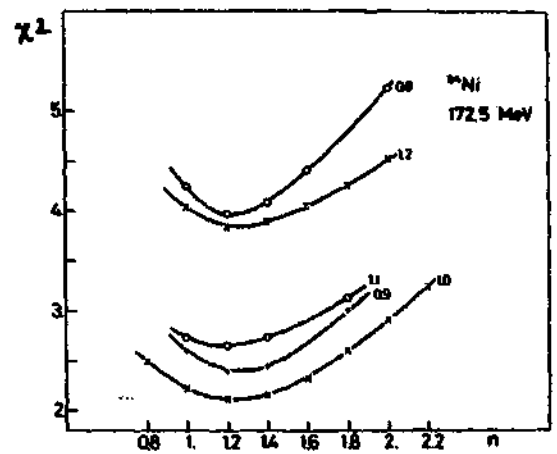

Fig. 4. The dependence of χ^2 on the power n in the case of ^{64}Ni. Various curves correspond to various normalizations.

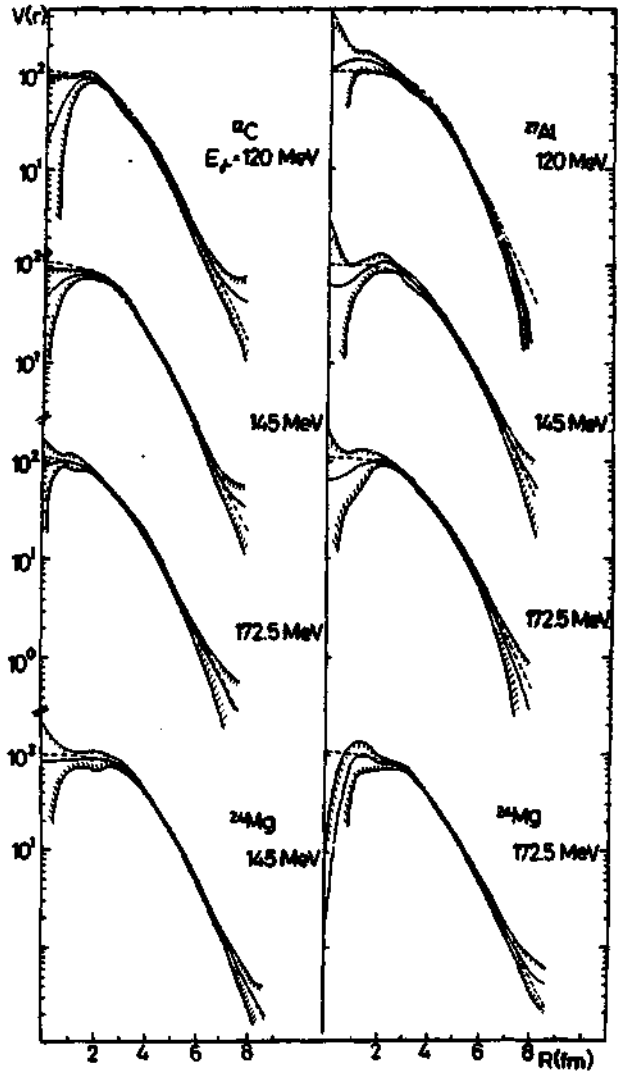

Fig. 5. The radial shapes of the potential V(r) found by the spline analysis. Shaded lines denote the limits of the error band and the dashed lines correspond to the WS form of V(r) calculated from the best fit parameters.